4

Functional Near Infrared Spectroscopy and Diffuse Optical Tomography in Neuroscience

Matteo Caffini[1], Davide Contini[1], Rebecca Re[1],
Lucia M. Zucchelli[1], Rinaldo Cubeddu[1],
Alessandro Torricelli[1] and Lorenzo Spinelli[2]
[1]*Dipartimento di Fisica - Politecnico di Milano, Milano*
[2]*CNR - Istituto di Fotonica e Nanotecnologie, Milano*
Italy

1. Introduction

Neuroimaging is the branch of medicine whose purpose is to provide visual information about the structure and the anatomy of the brain. The main techniques in clinics are: *Computed Tomography* (CT), *Magnetic Resonance Imaging* (MRI), *Diffuse Optical Tomography* (DOT), *Positron Emission Tomography* (PET) and *Single Photon Emission Computed Tomography* (SPECT).

CT scanning uses X-rays crossing the sample to image sections of the specimen in study. Specimen can be a living being, a part of if (e.g. the abdomen, a knee, the head, ...) or whatever non-living object. X-rays travel ballistically inside most of the materials (living tissue included), so measuring absorption of X-rays we can guess the composition of the sample we are measuring. Changing the direction of injection of the X-rays and merging absorption data coming from multiple directions makes a planar reconstruction of the examined section of the sample possible. CT is invasive in the sense that irradiates the patient with ionizing radiation. A little dose is given to the patient during a single CT session, anyway. CT scanning of the head is typically used to detect skull fractures, brain injuries, aneurysms, strokes, brain tumors and arteriovenous malformations in the brain.

MRI is based on nuclear magnetic resonance principles. It uses a strong static magnetic field to align the nuclear magnetization of hydrogen atoms of water in the body and then radio frequency fields are generated to alter this magnetization alignment. Several coils mounted on the scanner are then able to detect the magnetic field produced by the altered hydrogen atom magnetization and to relate the recovery time of these short-lasting magnetic fields to the environment in which resonant hydrogen atoms lie. MRI, using non-ionizing radiation, is generally considered non-invasive for the patient and provides greater contrast between different soft tissues than CT does. Magnetic resonance images of the head are mostly used to detect brain tumors.

PET and SPECT are nuclear medicine techniques and they are used in cancer localization. A radionuclide is injected in the body via blood flow and then tracked with detectors placed around the patient.

Functional neuroimaging is a particular way to perform medical neuroimaging focused more on functionality rather than just resolve anatomical features. The goal of functional neuroimaging is to detect *spatial* and *temporal* changes of activated areas of the brain, by measuring related physiological or physical features. The most common techniques are *functional Magnetic Resonance Imaging* (fMRI), *Electroencephalography* (EEG), *Magnetoencephalography* (MEG) and, recently, *functional Near InfraRed Spectroscopy* (fNIRS) and *Diffuse Optical Tomography* (DOT). PET and SPECT can be considered functional images as they use a radionuclide concentration to distinguish between healthy tissue and tumoral tissue.

Usually functional neuroimaging techniques are divided into two main classes: those with high spatial resolution ($\sim$ 1 cm or less) and those with high time resolution ($\sim$ 1 s or less).

- High spatial resolution and poor time resolution techniques (fMRI, PET and SPECT).
- High time resolution and poor spatial resolution techniques (EEG and MEG).

Having good time resolution and sufficient spatial resolution, DOT lays between the two classes and it is often considered the optimal compromise for functional neuroimaging studies. Spatial resolution in DOT is not an intrinsic feature, being the technique diffusion-limited. Nevertheless, in brain activation studies, integrating optical data and *a priori* anatomic data from MRI scans, brings to huge enhancements in spatial localization.

2. Functional near infraRed spectroscopy (fNIRS)

The simplest way to perform tissue oximetry using harmless electromagnetic radiation is to shine the tissue by means of a continuous beam of infrared light and to collect the re-emitted or transmitted light.

Hemoglobin is the key: oxygenated and deoxygenated states have considerably different absorption spectra and it turns out that, in first approximation, oxyhemoglobin and deoxyhemoglobin also are the two main chromophores in tissues into the InfraRed window. Because the underlining hypothesis states the presence of two chromophores, we need to inject radiation at two different wavelengths, possibly chosen where the spectra have the greatest differences (see Fig. 1). This spectroscopic technique uses constant light intensity and is known in literature as *Continuous Wave Near InfraRed Spectroscopy* (CW-NIRS) The most diffused wavelengths for CW-NIRS are 690 nm and 820 nm.

2.1 Absorption spectroscopy

Spectroscopy is the study of the interaction between radiation and matter, in particular absorption spectroscopy measures the absorption of radiation, in a selected range of frequency, in radiation-matter interaction. It is largely employed in analytical chemistry to check for the presence of elements or substances, being the absorption spectrum a sort of fingerprint and so characteristic of the substances. The simplest application is the detection of the amount of the substance present.

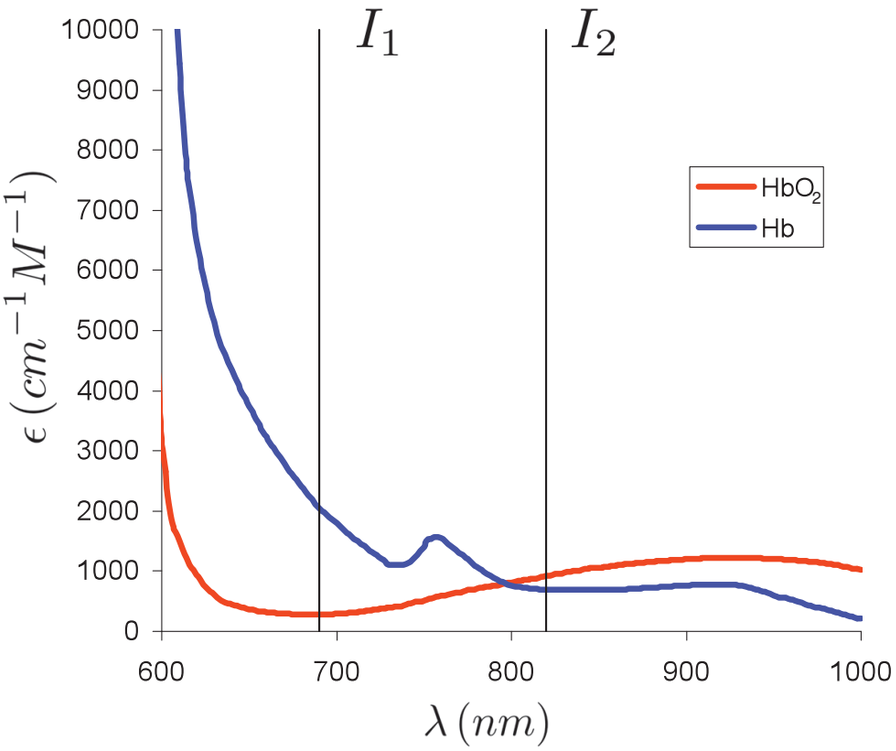

Fig. 1. The absorption spectrum, that is the molar extinction coefficient vs. the wavelength, of the oxygenated (red) and deoxygenated (blue) states of the hemoglobin. I_1 and I_2 are the chosen wavelengths for Near InfraRed Spectroscopy measurements.

When a radiation beam of known intensity I_0 crosses a layer of known width L of a certain medium (chromophore), part of the radiation is absorbed by the medium and the rest is transmitted on the other side of the layer (Fig. 2). Modeling this phenomenon supposing that each infinitesimal layer absorbs an amount of radiation dI and that this absorption is proportional to radiation intensity, brings to the following mathematical model. Calling μ_a the absorption coefficient and z the radiation beam direction, the radiation intensity I measured is modeled by the *Lambert-Beer law*:

$$\mathrm{d}I = -\mu_a I \mathrm{d}z \tag{1}$$

$$\int_{I_0}^{I} \frac{\mathrm{d}I}{I} = \int_0^L (-\mu_a)\,\mathrm{d}z \tag{2}$$

$$I = I_0 e^{-\mu_a L} \tag{3}$$

The absorption coefficient is measured in m^{-1} and has a straightforward interpretation: $l_a = \frac{1}{\mu_a}$ is the mean free path a photon travels prior to being absorbed. Moreover, it can be decomposed into two distinct factors: the absorbent medium concentration and its molar extinction coefficient ϵ:

$$\mu_a = [c]\,\epsilon \tag{4}$$

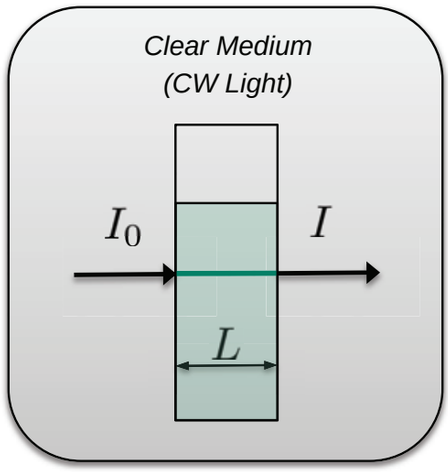

Fig. 2. Absorption Spectroscopy in the most simple geometry. Radiation is injected in the sample from one side and radiation intensity is measure on the other side. The Lambert-Beer law then allows to compute the chromophore concentration.

The extinction coefficient depends on the radiation wavelength: $\epsilon = \epsilon(\lambda)$ and so the absorption coefficient $\mu_a = \mu_a(\lambda)$. Such a functional dependence constitutes the *absorption spectrum* of the substance considered[1]. When more than a chromophore is present, each contribute is summed:

$$\mu_a = [c_1]\,\epsilon_1 + [c_2]\,\epsilon_2 + [c_3]\,\epsilon_3 + \cdots = \sum_i [c_i]\,\epsilon_i \tag{5}$$

Media for which this model holds are non-diffusing media, often called *clear media* and concentration measurements are easily conducted knowing the extinction coefficient of the chromophore and the length of the path traveled by the radiation. In the many chromophore experiment, performing multiple sessions, changing the radiation wavelength, allows to write a linear system and to obtain the unknown concentration of each chromophore.

Performing the same experiment described before using different media, it is found that for a vast class of substances this model is not accurate, as it doesn't take into account for the diffusion of radiation within the medium (Fig. 3(a)). Scattering events are due to discontinuities in dielectric properties of the medium and can be modeled as collisions between the photons of the radiation and particles in the medium. Many scattering models have been developed in physics: in classical electromagnetism by Rutherford, Thomson and Mie and in quantum physics by Compton and Raman [Feynman et al. (1964); Mie (1908); Rutherford (1911)]. A second important class of media then have to be described, media often called *turbid media*. Living tissues belong to this second class.

The Lambert-Beer model is still valid for this media, but the absorption coefficient alone is no more enough to describe the intensity drop found. A second coefficient μ_s, called *scattering*

[1] In many cases the absorption spectrum is given with respect to the frequency $\nu = \frac{c}{n\lambda}$, being c the speed of light and n the refraction index of the medium.

coefficient, is then introduced. The Lambert-Beer law it is written as follows:

$$I = I_0 e^{-(\mu_a + \mu_s)L} \tag{6}$$

The scattering coefficient here defined has a similar interpretation as the absorption coefficient: $l_s = \frac{1}{\mu_s}$ is the mean free path between two scattering events. Within this class of substances, absolute concentration measurements are possible only for thin samples (for thicker samples more complicated approaches are necessary, see section 2.3.1). Incidentally it can be noticed that this disturbing factor provides a helpful effect. Radiation scatters statistically in every direction, even backwards. It is then possible to collect radiation from the same side of the sample used for the radiation injection and to design experiments in reflectance geometry (Fig. 3(b)).

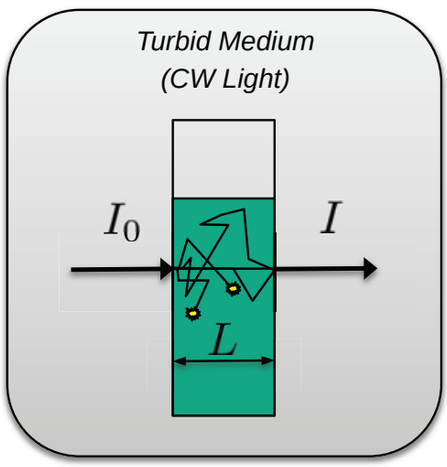

(a) Absorption Spectroscopy using a turbid medium does not allow to compute the chromophore concentration within the sample because of scattering contributes to intensity attenuation.

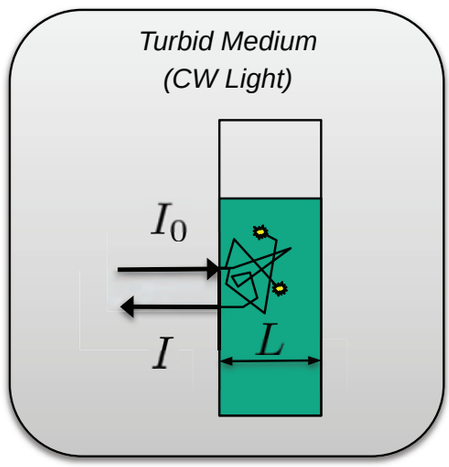

(b) When using turbid media experiments in reflection geometry are possible. Scattering provides a positive probability to have radiation traveling backwards after encountering scattering centers in the medium.

Fig. 3. Absorption spectrocopy in turbid medium in trasmission geometry (Fig. 3(a)) and reflection geometry (Fig. 3(b)).

A different approach is to irradiate the sample with a non-constant light intensity, but it becomes necessary to develop a more general model for light traveling inside turbid media. This will be done in section 2.3. First a simpler way to separate scattering contributes is explained.

In eq. 6 it has been seen that both absorption and scattering take part in the same way to radiation attenuation and that is not trivial to discriminate between the two distinct contributions. There's at least a case in which a simple way the separation is easily done. Suppose to have a medium in which the chromophore concentration $[c\,(t)]$ slightly varies in time and suppose to sample spectroscopic data in reflection geometry for a certain time interval. This case is not that far from reality as it may seem at first sight, for example in

biological tissues chromophores concentrations change in time because of blood flow. Then for each instant t_n a Lambert-Beer equation can be written as follow:

$$I(t_n) = I_0 e^{-([c(t_n)]\epsilon DL+G)} \tag{7}$$

where scattering contribution $\mu_s L$ has been grouped into the term G and the *differential pathlength factor* D has been introduced to take into account that photon travel paths longer than the source-detector separation because they penetrate inside the medium, scatters multiple times and then a little part reaches the detector traveling backwards. The differential pathlength factor depends only on the mean refractive index of the crossed medium. Hypothesizing that G doesn't vary in time and is constant for small variations of chromophore concentrations and introducing the physical quantity *absorbance* $A = \ln \frac{I}{I_0} = -([c]\,\epsilon DL + G)$, we can compute the variation in chromophore concentration between measurement collected at time t_n and time t_m in the following way:

$$\begin{aligned}
\Delta A_{mn} &= A_m - A_n && (8)\\
&= -c_m \epsilon DL - G + c_n \epsilon DL + G && (9)\\
&= -(c_m - c_n)\epsilon DL && (10)\\
&= -\Delta c_{mn} \epsilon DL && (11)
\end{aligned}$$

The scattering contributes vanishes and the variation in chromophore concentration depends only on the two intensity measurements collected:

$$\begin{aligned}
\Delta c_{mn} &= -\frac{\Delta A_{mn}}{\epsilon DL} && (12)\\
&= \frac{1}{\epsilon DL}(A_n - A_m) && (13)\\
&= \frac{1}{\epsilon DL}\left(\ln \frac{I_n}{I_0} - \ln \frac{I_m}{I_0}\right) && (14)\\
&= \frac{1}{\epsilon DL} \ln \left(\frac{I_n}{I_m}\right) && (15)
\end{aligned}$$

Most of times a reference measurement is conducted and all the concentration values are then computed as variation from the reference value.

2.2 Continuous wave NIRS (CW-NIRS)

Hemodynamic activity of the brain is related through metabolic processes to the electrical activity of the neurons, then, performing hemoglobin concentration measurements on the cortical tissues, it is possible to obtain information about spatial localization and temporal behavior of neuronal activity. The spectroscopic tools described in section 2.1 provide a straightforward way to do this. It is possible to inject radiation into the tissues and collect the photons coming out, for example using a reflectance geometry. The usefulness of

this technique would be to measure what happens within the blood flow, neglecting the contributes from the surrounding environment.

Collecting data at different times and then computing the absorbance variation values ΔA_{λ_1} and ΔA_{λ_2}, it is possible to write the following system of equations:

$$\begin{cases} \Delta A_{\lambda_1} = \left(\epsilon_{Hb,\lambda_1} \Delta\left[\mathrm{Hb}\right] + \epsilon_{\mathrm{HbO_2},\lambda_1} \Delta\left[\mathrm{HbO_2}\right]\right) D_{\lambda_1} L \\ \Delta A_{\lambda_2} = \left(\epsilon_{Hb,\lambda_2} \Delta\left[\mathrm{Hb}\right] + \epsilon_{\mathrm{HbO_2},\lambda_2} \Delta\left[\mathrm{HbO_2}\right]\right) D_{\lambda_2} L \end{cases} \tag{16}$$

In matrix form it becomes:

$$\begin{bmatrix} \frac{\Delta A_{\lambda_1}}{D_{\lambda_1} L} \\ \frac{\Delta A_{\lambda_2}}{D_{\lambda_2} L} \end{bmatrix} = \begin{bmatrix} \epsilon_{Hb,\lambda_1} & \epsilon_{\mathrm{HbO_2},\lambda_1} \\ \epsilon_{Hb,\lambda_2} & \epsilon_{\mathrm{HbO_2},\lambda_1} \end{bmatrix} \begin{bmatrix} \Delta\left[\mathrm{Hb}\right] \\ \Delta\left[\mathrm{HbO_2}\right] \end{bmatrix} \tag{17}$$

and finally:

$$\begin{bmatrix} \Delta\left[\mathrm{Hb}\right] \\ \Delta\left[\mathrm{HbO_2}\right] \end{bmatrix} = \begin{bmatrix} \epsilon_{Hb,\lambda_1} & \epsilon_{\mathrm{HbO_2},\lambda_1} \\ \epsilon_{Hb,\lambda_2} & \epsilon_{\mathrm{HbO_2},\lambda_1} \end{bmatrix}^{-1} \begin{bmatrix} \frac{\Delta A_{\lambda_1}}{D_{\lambda_1} L} \\ \frac{\Delta A_{\lambda_2}}{D_{\lambda_2} L} \end{bmatrix} \tag{18}$$

Being this a two equations systems with the two unknowns $\Delta\left[\mathrm{Hb}\right]$ and $\Delta\left[\mathrm{HbO_2}\right]$, a solution to the linear system is possible and the oxyhemoglobin and deoxyhemoglobin concentration variations with respect to a reference value can be computed (Eq. 18). If data are sampled for an interval of time, solving the linear system for each time sample, the time course of the concentrations is given.

Derived quantities such as total hemoglobin $\left[\mathrm{tHb}\right]$ are often plotted vs. time in order to improve the data visualization.

$$\Delta\left[\mathrm{tHb}\right] = \Delta\left[\mathrm{Hb}\right] + \Delta\left[\mathrm{HbO_2}\right] \tag{19}$$

An important limitation of CW-NIRS is the possibility to obtain just concentration variations. Having absolute concentration values, hemoglobin saturation $\mathrm{sO_2}$ could be calculated:

$$\mathrm{sO_2} = \frac{\left[\mathrm{HbO_2}\right]}{\left[\mathrm{tHb}\right]} \tag{20}$$

In principle there is no depth sensitivity with a single source-detector pair in CW-NIRS. Information on the composition of the media crossed by the CW light can be measured as an average. To increase light penetration large source-detector separation have been used (4-5 cm) with the obvious consequence of increasing the sampling volume and thus worsening the spatial resolution. Increasing the complexity of the system, the use of multi-source and multi-detector tomographic or topographic arrangements could overcome this limitation and better depth sensitivity [Boas et al. (2004); Strangman et al. (2002)].

Laboratory prototypes and commercial instrumentations have been developed through the years to measure oxygenation of the muscles and of the cortical regions of the brain. A comprehensive list can be found in Wolf et al. (2007).

2.3 Photon migration approach

A different way to deal with diffusion and discriminate between scattering and absorption contributes is to use non-constant light intensities in the injected radiation. A possible way to describe the physics of the problem is to start from the electric and magnetic fields associated with the radiation and to develop a rigorous mathematical theory, taking into account scattering, diffraction and interference. This is quite complicated, especially because of multiple scattering.

A more practical physical model of photon propagation into diffuse media based on energy flow is the *Radiative Transfer Equation* (RTE). This model was first developed to describe the non-interacting neutrons diffusion in nuclear reactors [Sanchez & McCormick (1982)]. The hypothesis of non-interacting particles reasonably applies to photons in multiple elastic scattering regime. The RTE model neglects polarization effects. This is not a problem though, because even if light coherence exists, this is going to be completely lost after a few scattering events.

2.3.1 The radiative transfer equation

The average power that at position $\boldsymbol{r}$ and time t flows through the unit area oriented in the direction of the unit vector $\hat{\boldsymbol{s}}$, due to photons within a unit frequency band centered at ν, that are moving within the unit solid angle around $\hat{\boldsymbol{s}}$ is the *spectral radiance* $I_s\left(\boldsymbol{r},\hat{\boldsymbol{s}},t,\nu\right)$. Thus at time t through the unit area $\mathrm{d}\Sigma$ lying in $\boldsymbol{r}$, oriented as $\hat{\boldsymbol{s}}$, within the unit solid angle $\mathrm{d}\Omega$ and in the frequency interval $[\nu,\nu+\mathrm{d}\nu]$ flows a power $\mathrm{d}P$ given by:

$$\mathrm{d}P = I_s\left(\boldsymbol{r},\hat{\boldsymbol{s}},t,\nu\right)\left|\hat{\boldsymbol{n}}\cdot\hat{\boldsymbol{s}}\right|\mathrm{d}\Sigma\mathrm{d}\Omega\mathrm{d}\nu \tag{21}$$

Energy density $\frac{\mathrm{d}E}{\mathrm{d}V}$ is simply related to spectral radiance. The energy $\mathrm{d}E$ per unit frequency and per unit solid angle that crossed the area $\mathrm{d}\Sigma$ oriented as $\hat{\boldsymbol{s}}$, in the time interval $\mathrm{d}t$ is:

$$\frac{\mathrm{d}E}{\mathrm{d}V} = \frac{I_s\mathrm{d}\Sigma\mathrm{d}t}{\mathrm{d}\Sigma v\mathrm{d}t} = \frac{I_s}{v} \tag{22}$$

Where v is the speed of radiation in the medium, $v=\frac{c}{n}$. Energy density is the number of photons and so I_s is proportional to the number of photons in the unit volume, with frequency ν, that at time t are moving in the direction $\hat{\boldsymbol{s}}$. As we deal with media in which the radiation frequency doesn't change during propagation (elastic scattering), we can integrate I_s over the frequency ν and obtain the *radiance* $I\left(\boldsymbol{r},\hat{\boldsymbol{s}},t\right)$.
Integrating also over the solid angle and dividing by v gives the quantity $u\left(\boldsymbol{r},t\right) = \frac{\int_{4\pi} I(\boldsymbol{r},\hat{\boldsymbol{s}},t)\mathrm{d}\Omega}{v}$, measured in $\left[\mathrm{Jm}^{-3}\right]$, that represents the energy density at position $\boldsymbol{r}$ and time t. Finally the photon density can be obtained dividing the energy density by the energy of a single photon:

$$n\left(\boldsymbol{r},t\right) = \frac{u\left(\boldsymbol{r},t\right)}{h\nu} \tag{23}$$

The RTE is an integro-differential equation stating the balance of the incoming and outgoing radiation along the direction $\hat{\boldsymbol{s}}$, at the time t, inside the volume element $\mathrm{d}V$ at the position $\boldsymbol{r}$

[Ishimaru (1978); Martelli et al. (2010)]:

$$\frac{1}{v}\frac{\partial I}{\partial t} = -\hat{\boldsymbol{s}}\cdot\nabla I - (\mu_a+\mu_s)\, I + \mu_s \int_{4\pi} p\left(\hat{\boldsymbol{s}},\hat{\boldsymbol{s}}'\right) I\left(\boldsymbol{r},\hat{\boldsymbol{s}}',t\right) \mathrm{d}\Omega' + q \tag{24}$$

Each term appearing has a precise significance:

- $\frac{1}{v}\frac{\partial I}{\partial t} \Rightarrow$ temporal change of energy.
- $-\hat{\boldsymbol{s}}\cdot\nabla I \Rightarrow$ change due to energy flow.
- $-(\mu_a+\mu_s)\, I \Rightarrow$ energy drop due to absorption and scattering.
- $+\mu_s \int_{4\pi} p\left(\hat{\boldsymbol{s}},\hat{\boldsymbol{s}}'\right) I\left(\boldsymbol{r},\hat{\boldsymbol{s}}',t\right) \mathrm{d}\Omega' \Rightarrow$ energy gain from radiation coming from every direction, but scattered into the direction $\hat{\boldsymbol{s}}$, being $p\left(\hat{\boldsymbol{s}},\hat{\boldsymbol{s}}'\right)$ the *phase function*, that is the probability that a photon flowing in the direction $\hat{\boldsymbol{s}}$ is scattered into the direction $\hat{\boldsymbol{s}}'$.
- $q = q\left(\boldsymbol{r},\hat{\boldsymbol{s}},t\right) \Rightarrow$ Radiation source inside $\mathrm{d}V$ $\left[\mathrm{Wm}^{-3}\mathrm{sr}^{-1}\right]$.

The RTE has two immediate properties:

1. If I_0 is a solution for a non-absorbing medium with time impulsive source term $q\left(\boldsymbol{r},\hat{\boldsymbol{s}},t\right) = q_0\left(\boldsymbol{r},\hat{\boldsymbol{s}}\right)\delta\left(t\right)$, then if the absorption coefficient is μ_a the solution is:

$$I = I_0 e^{-\mu_a v t} \tag{25}$$

   This property is a generalization of the Lambert-Beer law [Sassaroli & Fantini (2004); Tsuchiya (2001)].

2. If I is the Green function for a medium having extinction coefficient $\mu_t = \mu_a + \mu_s$ and albedo $a = \frac{\mu_s}{\mu_t}$, then for a medium having extinction coefficient μ_t^* and the same albedo, the solution is scaled in this way:

$$I\left(\boldsymbol{r^*},\hat{\boldsymbol{s}},t^*\right) = \left(\frac{\mu_t^*}{\mu_t}\right)^3 I\left(\boldsymbol{r},\hat{\boldsymbol{s}},t\right) \qquad \begin{cases} \mathbf{r}^* = \left(\frac{\mu_t}{\mu_t^*}\right)\mathbf{r} \\ t^* = \left(\frac{\mu_t}{\mu_t^*}\right) t \end{cases} \tag{26}$$

   This scaling property is known as the *similarity principle* [Zege et al. (1991)].

Because of the high complexity of the RTE, no analytical solutions are available and approximation methods are then applied. Numerical methods like the *Finite Difference Method* or the *Finite Elements Method* (FEM) require a large amount of computational power, but are often applied [Arridge (1995); Arridge et al. (2000); Arridge & Hebden (1997); Arridge & Schweiger (1995); Arridge et al. (1993)]. Stochastic methods like the *Monte Carlo* are widely used in many biological applications [Boas et al. (2002); Fang & Boas (2009)].

2.3.2 The $\mathbf{P_N}$ approximation

Many ways to simplify the RTE have been developed through the years, but most methods are based on the P_N *approximation*. Two derived quantities of interest are the *photon fluence* Φ

and the *photon flux* $\boldsymbol{J}$:

$$\Phi(\boldsymbol{r},t) = \int_{4\pi} I(\boldsymbol{r},\hat{\boldsymbol{s}},t)\,\mathrm{d}\Omega \tag{27}$$

$$\boldsymbol{J}(\boldsymbol{r},t) = \int_{4\pi} I(\boldsymbol{r},\hat{\boldsymbol{s}},t)\,\hat{\boldsymbol{s}}\mathrm{d}\Omega \tag{28}$$

Radiance and source term are expanded in spherical harmonics [Boas (1996); Jackson (1999)]:

$$I(\boldsymbol{r},\hat{\boldsymbol{s}},t) = \sum_{l=0}^{+\infty}\sum_{m=-l}^{l}\sqrt{\frac{2l+1}{4\pi}}\phi_{l,m}(\boldsymbol{r},t)\,Y_{l,m}(\hat{\boldsymbol{s}}) \tag{29}$$

$$q(\boldsymbol{r},\hat{\boldsymbol{s}},t) = \sum_{l=0}^{+\infty}\sum_{m=-l}^{l}\sqrt{\frac{2l+1}{4\pi}}q_{l,m}(\boldsymbol{r},t)\,Y_{l,m}(\hat{\boldsymbol{s}}) \tag{30}$$

Phase function is expanded in spherical harmonics too, but first the reasonable hypothesis that the scattering amplitude is only dependent on the change in direction of the photon is made. With this assumption the probability of scattering from a direction $\hat{\boldsymbol{s}}$ into a direction $\hat{\boldsymbol{s}}'$ depends only on the angle between $\hat{\boldsymbol{s}}$ and $\hat{\boldsymbol{s}}'$:

$$p(\hat{\boldsymbol{s}}\cdot\hat{\boldsymbol{s}}') = \sum_{l=0}^{+\infty}\frac{2l+1}{4\pi}g_l P_l(\hat{\boldsymbol{s}}\cdot\hat{\boldsymbol{s}}') \tag{31}$$

$$= \sum_{l=0}^{+\infty}\sum_{m=-l}^{l} g_l Y^*_{l,m}(\hat{\boldsymbol{s}}')\,Y_{l,m}(\hat{\boldsymbol{s}}) \tag{32}$$

Where P_l is the Legendre polynomial of order l and the angular addition rule has been used [Jackson (1999)]. The normalization factors $\sqrt{\frac{2l+1}{4\pi}}$ and $\frac{2l+1}{4\pi}$ are introduced for convenience.

Truncating the series at the $l = N$ term brings to the P_N approximation of the RTE [Arridge (1999)]. In the P_1 approximation the radiance[2], source and phase function reduce to:

$$I(\boldsymbol{r},\hat{\boldsymbol{s}},t) = \frac{1}{4\pi}\Phi(\boldsymbol{r},t) + \frac{3}{4\pi}\boldsymbol{J}(\boldsymbol{r},t)\cdot\hat{\boldsymbol{s}} \tag{33}$$

$$q(\boldsymbol{r},\hat{\boldsymbol{s}},t) = \frac{1}{4\pi}q_0(\boldsymbol{r},t) + \frac{3}{4\pi}\boldsymbol{q_1}(\boldsymbol{r},t)\cdot\hat{\boldsymbol{s}} \tag{34}$$

$$p(\hat{\boldsymbol{s}}\cdot\hat{\boldsymbol{s}}') = \frac{1}{4\pi}g_0 + \frac{3}{4\pi}g_1\hat{\boldsymbol{s}}\cdot\hat{\boldsymbol{s}}' \tag{35}$$

Where we used the definition of fluence 27 and flux 28, obtaining:

$$\Phi(\boldsymbol{r},t) = \phi_{0,0}(\boldsymbol{r},t) \tag{36}$$

$$\boldsymbol{J}(\boldsymbol{r},t) = \begin{pmatrix} \frac{1}{\sqrt{2}}\left(\phi_{1,-1}(\boldsymbol{r},t) - \phi_{1,1}(\boldsymbol{r},t)\right) \\ \frac{1}{i\sqrt{2}}\left(\phi_{1,-1}(\boldsymbol{r},t) + \phi_{1,1}(\boldsymbol{r},t)\right) \\ \phi_{1,0}(\boldsymbol{r},t) \end{pmatrix} \tag{37}$$

[2] As will be realized soon, this brings to assume the radiance to be nearly isotropic. This is a good approximation for biological tissues and in general for high-albedo media, because of the few absorption events relative to the scattering events.

For the source term approximation the quantities monopole moment q_0 and dipole moment $\boldsymbol{q_1}$ have been introduced:

$$q_0(\boldsymbol{r},t) = q_{0,0}(\boldsymbol{r},t) \tag{38}$$

$$\boldsymbol{q_1}(\boldsymbol{r},t) = \begin{pmatrix} \frac{1}{\sqrt{2}}\left(q_{1,-1}(\boldsymbol{r},t) - q_{1,1}(\boldsymbol{r},t)\right) \\ \frac{1}{i\sqrt{2}}\left(q_{1,-1}(\boldsymbol{r},t) + q_{1,1}(\boldsymbol{r},t)\right) \\ q_{1,0}(\boldsymbol{r},t) \end{pmatrix} \tag{39}$$

Normalizing g_0 to unity, g_1 is the average cosine of the scattering angle:

$$g_0 = 1 \tag{40}$$

$$g_1 = <\hat{\boldsymbol{s}}\cdot\hat{\boldsymbol{s}}'> \tag{41}$$

Finally, substituting these approximated expressions into 24, we obtain:

$$\frac{1}{v}\frac{\partial\Phi(\boldsymbol{r},t)}{\partial t} = -\mu_a\Phi(\boldsymbol{r},t) - \nabla\cdot\boldsymbol{J}(\boldsymbol{r},t) + q_0(\boldsymbol{r},t) \tag{42}$$

$$\frac{1}{v}\frac{\partial\boldsymbol{J}(\boldsymbol{r},t)}{\partial t} = -\left(\mu_a+\mu_s'\right)\boldsymbol{J}(\boldsymbol{r},t) - \frac{1}{3}\nabla\Phi(\boldsymbol{r},t) + \boldsymbol{q_1}(\boldsymbol{r},t) \tag{43}$$

Where we made use of the definition of reduced scattering coefficient μ_s':

$$\mu_s' = (1-g_1)\,\mu_s \tag{44}$$

2.3.3 The diffusion approximation

In a high-albedo (predominantly scattering) medium, the time for a substantial change in flux $\boldsymbol{J}$ is much longer than the time to traverse one transport mean free path. Thus, over one transport mean free path itself, the fractional change in flux is much less than unity. The *diffusion approximation* results from making the following assumptions:

$$\frac{\partial\boldsymbol{J}(\boldsymbol{r},t)}{\partial t} = 0 \tag{45}$$

$$\boldsymbol{q_1}(\boldsymbol{r},t) = 0 \tag{46}$$

Dropping the dipole moment of the source is reasonable assuming an isotropic source. Eq. 43 then becomes *Fick's law*:

$$\boldsymbol{J}(\boldsymbol{r},t) = -\frac{1}{3\left(\mu_a+\mu_s'\right)}\nabla\Phi(\boldsymbol{r},t) \tag{47}$$

Usually the factor multiplying the gradient is called *diffusion coefficient*, $D = \frac{1}{3(\mu_a+\mu_s')}$. We notice that in high-albedo medium ($\mu_s' \gg \mu_a$) it doesn't depend on absorption and can be calculated as $D \approx \frac{1}{3\mu_s'}$[3].

[3] This is consistent with the similarity principle previously introduced [Martelli et al. (2010)].

Substituting into Eq. 42 we finally have the *diffusion equation* (DE):

$$\frac{1}{v}\frac{\partial\Phi(\boldsymbol{r},t)}{\partial t} = -\mu_a\Phi(\boldsymbol{r},t) + \nabla\cdot D\nabla\Phi(\boldsymbol{r},t) + q_0(\boldsymbol{r},t) \tag{48}$$

The diffusion equation models many problems in Physics and Chemistry, such as heat propagation, ion diffusion and semiconductor doping. Analytical solution to the DE in photon migration have been carried out in symmetrical geometries such as the infinite medium, the semi-infinite medium or the semi-infinite medium with a high-absorbent inclusion.

In order to solve the DE, appropriate boundary conditions have to be declared. The most general boundary condition is the *Partial Current Boundary Condition* (PCBC):

$$\Phi(\boldsymbol{r},t) + 2AD\nabla\Phi(\boldsymbol{r},t)\cdot\hat{\boldsymbol{n}} = 0 \qquad \boldsymbol{r}\in\partial V \tag{49}$$

Where A is a coefficient depending on the refractive index and is due to Fresnel reflection [Contini et al. (1997); Martelli et al. (2010)]. In practical applications, though, the most commonly applied boundary conditions are the *Extrapolated Boundary Condition* (EBC) and the *Zero Boundary Condition* (ZBC):

$$\Phi(\boldsymbol{r},t) = 0 \qquad \boldsymbol{r}\in\partial V_{ext} \tag{50}$$

$$\Phi(\boldsymbol{r},t) = 0 \qquad \boldsymbol{r}\in\partial V \tag{51}$$

Where ∂V_{ext} is a surface distant $2AD$ from the boundary (extrapolated surface).

CW, TR and FD solutions for simple geometries have been calculated [Martelli et al. (2010)].

2.3.4 FD-NIRS

Frequency Domain Near InfraRed Spectroscopy (FD-NIRS) makes use of intensity modulated laser light (typically at radio frequencies), injecting it into the sample. The remitted wave is demodulated to obtain amplitude and phase as a function of the modulation frequency. The tissue acts like a low-pass filter: the amplitude is a decreasing function of the frequency and the phase typically increases. The analytical expressions for amplitude and phase can be obtained by a Fourier transform of the TR theoretical expression. Estimation of optical properties can thus be performed using the photon migration theory (see Fig. 4).

Some commercial device using frequency domain techniques is available and measurements and basic research often used this approach to study biological tissues oxygenation [D'Arceuil et al. (2005); Fantini et al. (1995)].

2.3.5 TR-NIRS

In section 2.2 a way to measure oxygenated and deoxygenated hemoglobin concentrations has been described. Using absorption spectroscopy techniques it is possible to investigate *in vivo* the oxygenation status of the superficial tissues and in particular of the cortical areas of the brain. Thus, CW-NIRS is a useful non-invasive technique for functional neuroimaging. As previously seen, the issue underlying Near InfraRed Spectroscopy is scattering. The way CW-NIRS deals with scattering is to perform a basal measurement and then to refer all

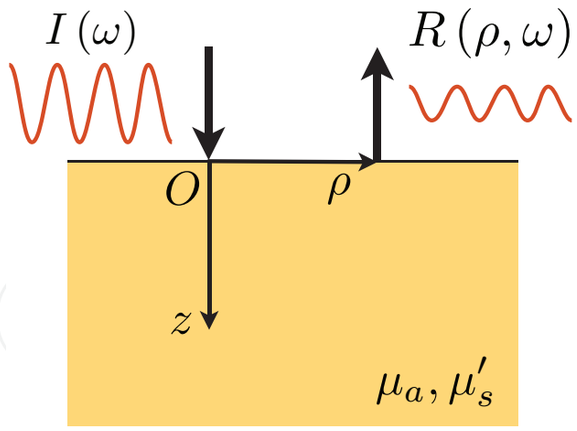

Fig. 4. Scheme of reflection geometry FD-NIRS measurement. Intensity modulated light $I(\omega)$ travels in the medium and part of it can be collected by a detector at a source-detector distance ρ. Amplitude and phase of the collected light $R(\rho,\omega)$ depend on μ_a and μ_s'.

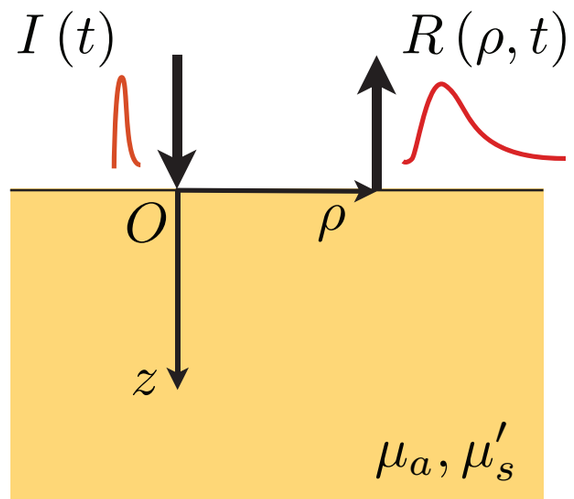

Fig. 5. Scheme of reflection geometry TD-NIRS measurement. Injected light travels in the medium and part of it can be collected by a detector at a source-detector distance ρ. Knowing the temporal shape of the injected light $I(t)$, the temporal shape of the collected light $R(\rho,t)$ depends on μ_a and μ_s'.

successive data to the baseline values, making the assumption that scattering is constant in time. This makes concentration variations the only possible obtainable data.

In section 2.3.1 the physical model for radiation propagation inside tissues has been introduced. It will be now shown how RTE gives a practically useful tool to perform a kind of measurement in which absolute hemoglobin concentrations values can be sampled.

In many biological applications the semi-infinite geometry is assumed and light intensity measurement are conducted in reflectance geometry (see Fig. 5). In this case the Green function of the Diffusion Equation with the Extrapolated Boundary Condition, expressed as

the detected power per unit area (usually known as *reflectance R*), takes the form:

$$R(\rho,t)=\frac{1}{2\left(4\pi Dv\right)^{3/2}t^{5/2}}e^{-\frac{\rho^2}{4Dvt}}e^{-\mu_a vt}\left[z_0e^{-\frac{z_0^2}{4Dvt}}-z_pe^{-\frac{z_p^2}{4Dvt}}\right] \tag{52}$$

Where ρ is the source-detector distance, $z_0=\frac{1}{\mu_s'}$, $z_p=z_0+2z_e$ and $z_e=2AD$.

Looking at the the Green function of the diffusion equation it is possible to notice that absorption and scattering contributes are naturally separated in the model. Plotting these solutions for different values of the absorption coefficient and of the scattering coefficient evidence this property (see Fig. 6). This technique based on the injection of light with a known temporal shape (typical a pulse-like shape) and the estimation of the optical properties from the emitted light temporal shape is called *Time-Resolved Near InfraRed Spectroscopy* (TR-NIRS).

The light is collected by means of photomultipliers tubes (PMT) or avalanche photodiodes (APD) usually in Time Correlated Single Photon Counting (TCSPC) regime. Detailed descriptions of the way light is collected by light detectors is given in [Donati (1998)] and of TCSPC is given in [O'Connor & Phillips (1984)] and [Becker (2005)].

Estimation of the optical properties can be performed from all the analytical expressions for the TR response of a diffusive medium. Absorption and scattering coefficients can be computed by means of an inversion algorithm [Press et al. (1992)]. The instrumental response function (IRF) due to temporal dispersion in fiber, temporal jitter of detectors and finite pulse width of light sources has to be taken into account. Due to the linearity and time-invariance of the transport problem, the detected response is the convolution between the IRF and the theoretical response of the medium. Thus, a Levenberg-Marquardt non-linear minimization between experimental data and theoretical curve convoluted with the IRF is generally performed.

An estimation of the optical properties of a diffusive medium can be also performed by means of Monte Carlo simulations. A certain number of simulations are needed, then by using the scaling properties of the RTE it is possible to implement a fast search of the correct simulation [Pifferi et al. (1998)]. These two method enable an absolute estimation of optical properties.

A simple estimation of the variation of the absorption coefficient can be easily performed if only absorption changes are assumed (and usually are). If we collect at different times two reflectance curves $R_0(\rho,t)$ and $R_1(\rho,t)$, it is straightforward that:

$$\Delta\mu_a=-\frac{1}{vt}\ln\left(\frac{R_1(\rho,t)}{R_0(\rho,t)}\right) \tag{53}$$

In principle TR techniques provides a richer insight than CW to the problem of non-invasively probing of a diffusive medium. These approaches can discriminate between absorption and scattering contributions and derive absolute values for the hemodynamic parameters [Patterson et al. (1989)]. This however can be obtained only in simple geometries like the infinite or the semi-infinite homogeneous models. In a real heterogeneous medium like the human tissues and in particular the human head it is easier to derive changes with respect to a baseline or effective average parameters rather than absolute values. Advanced time-resolved

perturbation models for more complicated geometries, like multi-layered media, have been derived in the last years, but they would require the use of a priori information (e.g., the

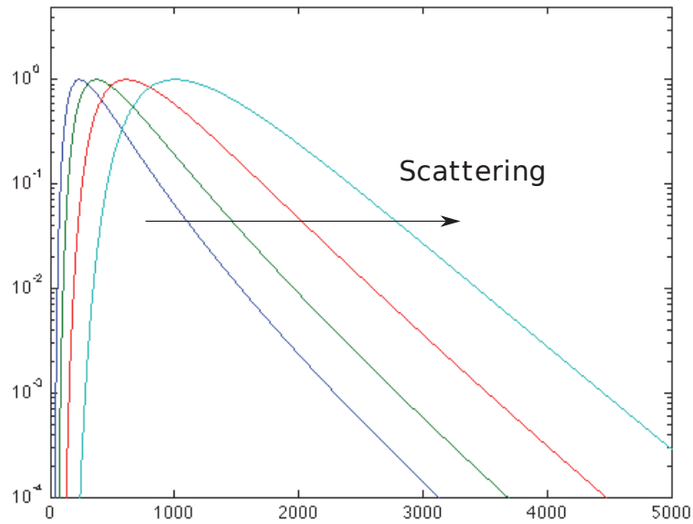

(a) Dependance from scattering ($\mu_a = 0.09$ cm^{-1}, μ_s' =4, 8, 16, 32 cm^{-1}).

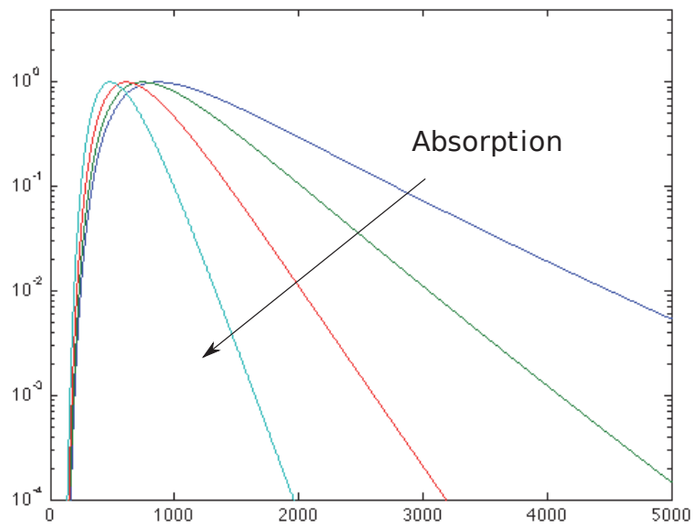

(b) Dependance from absorption ($\mu_a = 0.04, 0.08, 0.16, 0.32$ cm^{-1}, $\mu_s' = 20$ cm^{-1}).

Fig. 6. Normalized reflectance from the semi-infinite model, with source-detector distance ρ=2 cm. Reflectance vs. time is plotted in semi-logarithmic scale.

anatomy of the head as provided by a MRI scan) for their practical and effective use [Martelli et al. (2005)].

The actual potentiality of time-resolved techniques relies on an easier approach to the problem of depth sensitivity. As mentioned before, to enhance depth sensitivity, CW systems use large source-detector distance and multi-distance approaches. Conversely, depth sensitivity in TR-NIRS can be intrinsic in the measured reflectance curve having information on the time of flight of the photons in tissues.

Near InfraRed Spectroscopy applications to the brain spread from rehabilitation monitoring to neural plasticity studies, from localization of cortical activation in motor or cognitive tasks to stroke diagnosis, and more. Motor tasks such as finger tapping or hand grasping are easy to perform and hundreds of studies have been published [Torricelli et al. (2007)]. Cognitive tasks present more difficulties in activation interpretation, nevertheless a number of study is available in literature [Bandettini et al. (1997); Butti et al. (2009); Heekeren et al. (1997)]. Fig. 7 and Fig. 8 show two examples of TR-NIRS data.

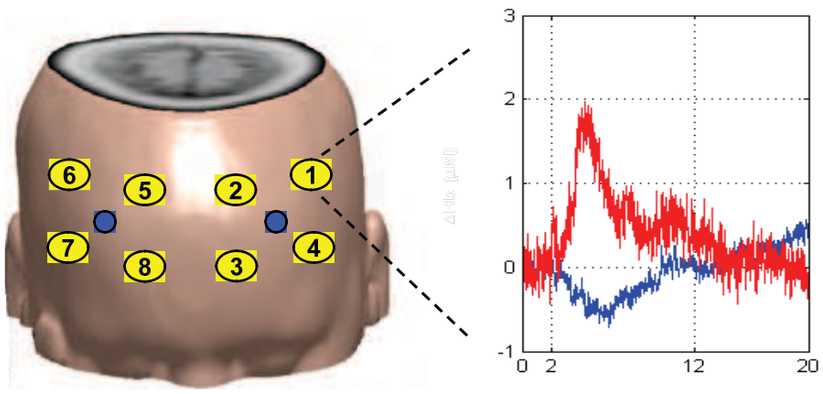

Fig. 7. Δ [Hb] (blue) and Δ [HbO_2] (red) concentrations (in arbitrary units) vs. time (in minutes) collected from the frontal area of the brain during a cognitive task of sustained attention. Vertical lines indicated the beginning and the end of the task. The average concentration value for the first two minutes block was used as baseline and then subtracted to all data.

3. Diffuse Optical Tomography (DOT)

Since the very beginning of the history of NIRS, many efforts have been made to improve space resolution and data accuracy. Near InfraRed Spectroscopy provides functional information about the oxygenation status of the explored tissues, but a single source-detector pair is only able to probe a small underlying area. In this section a way to perform functional neuroimaging starting form NIRS data will be introduced. Production of two dimensional maps, often called *topography*, by linear interpolation of NIRS data was the first application to be investigated. This imaging technique is usually called *Diffuse Optical Imaging* (DOI) and, adding depth sensitivity, is known as *Diffuse Optical Tomography* (DOT).

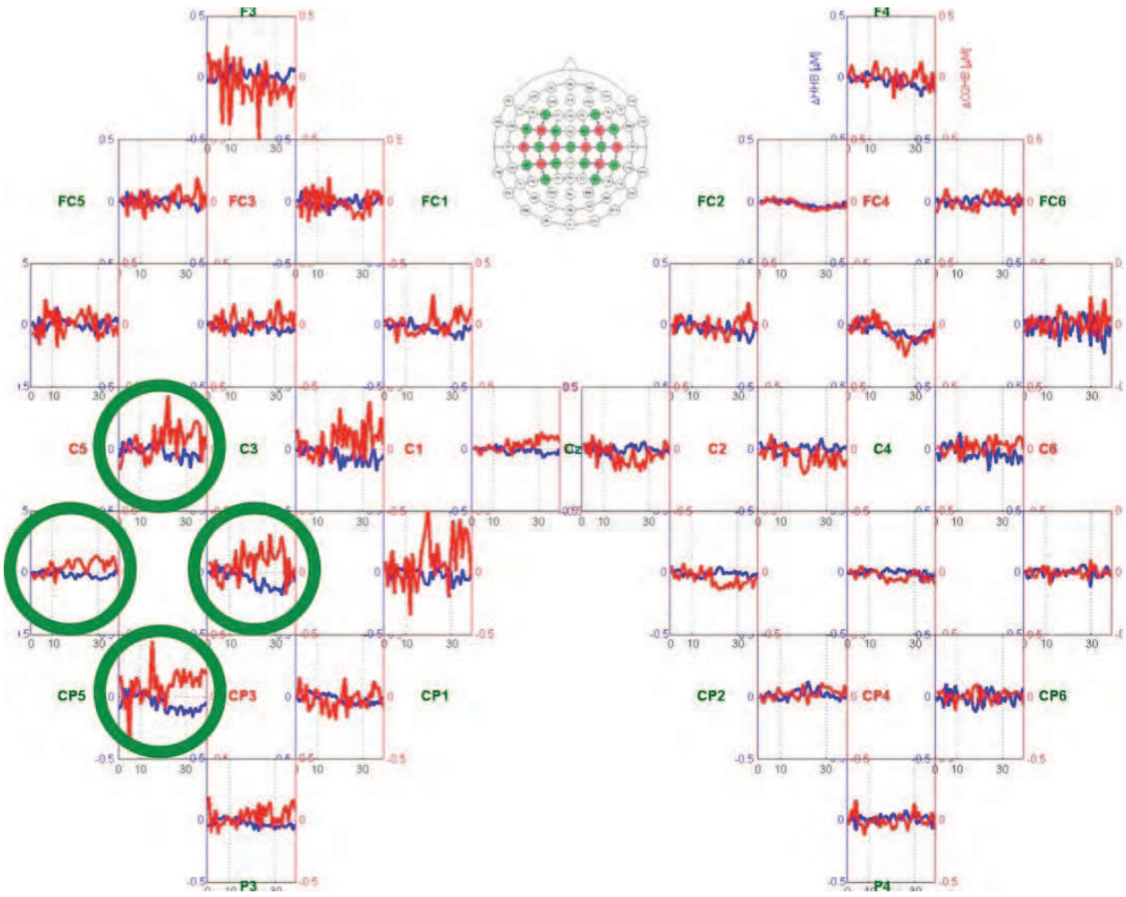

Fig. 8. Oxyhemoglobin (in red) and deoxyhemoglobin (in blue) concentrations for a hand grasping task. Single-subject, right hand movement, average of 10 repetitions, TR-NIRS device, contrast enhanced for the deep layers (see section 3.1).

To properly investigate a large area (larger than the common source-detector distance, that is 1-4 cm) a multi-channel approach is needed. The starting point is the arrangement of a number of sources and detectors to cover the area of interest and the management of the source-detector pairs. Depending on the physical dimensions of the area even a huge number could be arranged. No theoretical limitations on the number of optodes exists, however, actual technology features instrumentations with up to 32 sources and 32 detectors (CW) and 16 sources and 16 detection channels (TR). Shining NIR light on the skin and collecting the back-scattered light in a reflectance geometry from multiple points easily allows to draw a map of the hemoglobin concentrations around the area of interest. Spatial resolution is poor (depending on source-detector distances) and a little depth sensitivity (associated to the overlapping measurements in CW or intrinsic in TR) is obtained.

Concentrations time series can be plotted vs time or a spatial map can be built (see Fig. 9). A movie-like map can be obtained if each frame corresponds to a time sample. More often, especially in books and publications, averaged concentrations data over time intervals are used to obtain maps relative to a time block of seconds or minutes, just as the example in Fig 9.

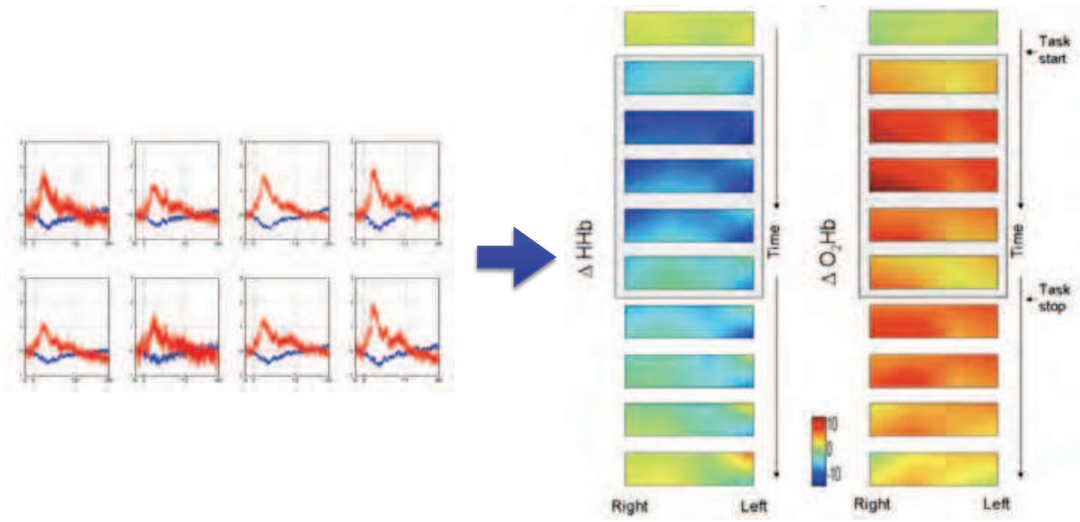

Fig. 9. The concentration time series can be visualized as spatial map. Each time sample belongs to an average position between the associated source-detector pair. The map is built by linear interpolation with the neighboring points concentration values.

More complicated ways to image optical data have been developed. Using MRI anatomical information and using suitable values for the average optical properties of the tissues a inverse problem can be established. Localized alterations of the optical properties, corresponding to a increased absorption and related to the hemodynamic responses of neural activations, can be put in correspondence with cortical features and a better localization of brain activations can be performed.

DOT systems can consist of little more than a probe with fiber-optic sources and detectors, a piece of dedicated hardware about the size of a small suitcase and a laptop computer. Systems can be much larger, depending primarily on the type of laser source and detectors employed, but the approach generally offers a degree of portability unobtainable with many other modalities. For this reason, looking into the future, DOT may be ideally suited for clinical applications such as bedside monitoring of cerebral oxygenation.

3.1 Time resolved DOT

A fundamental point in NIRS measurements, whatever technique we are using, is the ability to separate systemic hemodynamic changes occurring in the superficial tissues, such as the skin, from functional hemodynamic changes related to brain activations. In order to reach this goal is fundamental to discuss NIRS depth sensitivity. Depth sensitivity is not intrinsic in CW- and TR-NIRS measurements, but can be achieved using proper optodes configurations or using time of flight information. Multi-distance source-detector approaches, both with CW [Saager & Berger (2005)] and with TR [Liebert et al. (2004)] techniques, have been proposed to improve depth selectivity and sensitivity. Single-distance approaches have also been discussed [Selb et al. (2005); Steinbrink et al. (2001)]. Contini et al. (2007) proposed a different approach to add depth information to the tissue probing problem, based on time-domain contrast functions. Wabnitz et al. (2008) discussed a method for depth selectivity based on time windows and moments of time-of-flight distributions for TD-NIRS.

Time-resolved curves statistically contain information about tissues which light photons pass through. Photons reaching the detector at early times surely have been back-scattered from the superficial tissues and thus can bring information about the superficial layers only. Photons reaching the detector at late times have travelled inside the tissues for a longer time and statistically could have probed deeper layers and carry information about them. We usually refer to them as *early photons* and *late photons*.

A simple approach to the depth probing problem could be to develop a contrast function, considering just two domains: superficial layers and deep layers.

In order to develop models to discriminate between the variations of the absorption coefficient in the superficial layers ($\Delta\mu_a^{UP}$) and of the variation of the absorption coefficient in deep layers ($\Delta\mu_a^{DOWN}$), the quantity time-dependent photon path length, usually called Mean time-dependent Path Length (MPL) is introduced [Steinbrink et al. (2001)]. As its own name suggests, MPL is the average length of the path travelled by photons in a specific layer and can be calculated from the mean time of flight of the photons.

The reflectance curve is divided into time intervals τ, called *time gates* (TG), and the total counts (usually referred as *intensity*) are calculated for each time gate[4].

Being $I_0(t)$ the intensity for the non-absorbent medium, $L^{UP}(t)$ and $L^{DOWN}(t)$ the mean time-dependent path lengths in the superficial layers and in the deep layers, respectively, the expression for the intensity $I(t)$ in a general absorbent medium can be expressed as:

$$I(t) = I_0(t)\, e^{-\left(\Delta\mu_a^{UP} L^{UP}(t) + \Delta\mu_a^{DOWN} L^{DOWN}(t)\right)} \tag{54}$$

In the simplest case, it is possible to think that early photons carry information only about the superficial layers and that late photons are not affected by a superficial inhomogeneity, and carry information only about the deep layers. Thus, we can write for the absorption coefficient changes:

$$\Delta\mu_a^{UP} = -\frac{1}{L^{UP}(\tau_e)} \ln\left(\frac{I(\tau_e)}{I_0(\tau_e)}\right) \tag{55}$$

$$\Delta\mu_a^{DOWN} = -\frac{1}{L^{DOWN}(\tau_l)} \ln\left(\frac{I(\tau_l)}{I_0(\tau_l)}\right) \tag{56}$$

where τ_e is the mean time of flight of photons in a early time gate and τ_l is the mean time of flight for photons in a late time gate. Despite giving a general idea about how to obtain information about contributes of different layers, this model is pretty rough, indeed. The hypothesis of late photons not affected by superficial layers has to be rejected and more complicated expressions are often necessary to perform depth selection [Contini (2007)]. It can be proved that late photons carry both information about superficial and deep layers and that superficial layer absorption variations affect the deep layers absorption estimation. The subtraction of the superficial contribute is thus necessary in the estimation of $\Delta\mu_a^{DOWN}$. Such

[4] The total counts are the time integral of the reflectance curve: $I_{gate}(t) = \int_{t_{in}}^{t_{fin}} R(t)\, \mathrm{d}t$

a subtraction can be performed as follow:

$$\Delta\mu_a^{UP} = -\frac{1}{L^{UP}(\tau_e)} \ln\left(\frac{I(\tau_e)}{I_0(\tau_e)}\right) \tag{57}$$

$$\Delta\mu_a^{DOWN} = -\frac{1}{L^{DOWN}(\tau_l)} \ln\left(1 + \frac{I(\tau_l)}{I_0(\tau_l)} - \frac{I(\tau_e)}{I_0(\tau_e)}\right) \tag{58}$$

Oxy- and deoxy-hemoglobin concentrations for the upper layer and the lower layer can be easily obtained via Lambert-Beer law, from the estimated $\Delta\mu_a$. An example of application of this stratigraphic model is shown in Fig. 10, where data where collected during a Valsalva maneuver, that forces an increase of the systemic blood volume, resulting in an increase of both oxyhemoglobin and deoxyhemoglobin concentrations in the superficial layers of the skin.

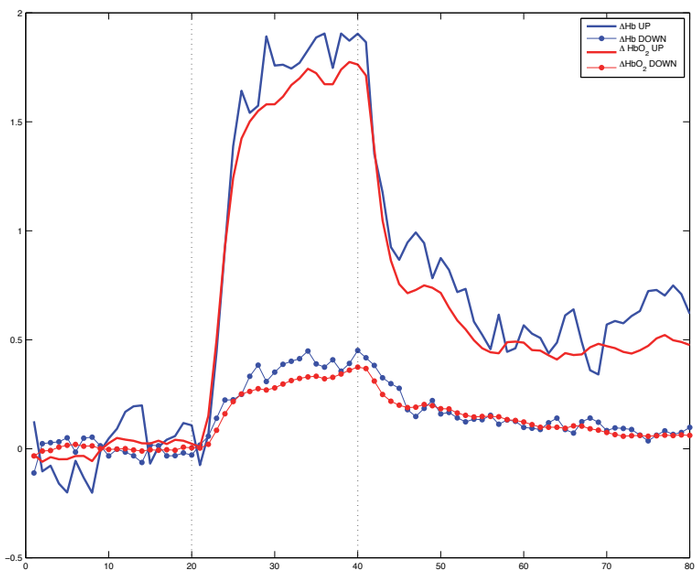

Fig. 10. Estimated ΔHbO_2 and ΔHb in the superficial layer (UP, continuous line) and in the brain (DOWN, dotted line) during the Valsalva maneuver without normalization. The two vertical dashed lines indicate the beginning and the end of the task period, respectively. During the Valsalva maneuver the sistemic blood volume dramatically increases, while the local blood volume in the brain is less affected by the maneuver effects. A proper depth selectivity remarks this differences.

3.2 Multimodality approach

Recently a great interest in multimodality approaches has grown. Merging the advantages of different imaging and functional techniques, such as co-registration of NIRS with MRI [Merritt et al. (2002)], blood flow monitors, fMRI [Torricelli et al. (2007)] and PET, gives the possibility to build anatomo-functional images and movies to largely improve information visualization.

Moreover, the comparison with standard clinical techniques such EEG or MEG can lead to a clinical standardization of the NIRS signal and push Near InfraRed Spectroscopy towards a regular clinical use [*nEUROPt Project* (2008-2012)].

Using anatomical magnetic resonance priors to perform MRI-guided optical reconstruction dramatically improves the spatial resolution of the diffuse optical tomography techniques [Boas & Dale (2005)]. Simulations of light propagation are run into the MRI head volume, using Monte Carlo statistical methods such as Fang & Boas (2009), and then the cortical activation profile is obtained solving an inverse problem. For a more detailed description of it see Caffini et al. (2011).

In the event of an unavailability of the subject-specific anatomy the efficient use of an MRI anatomical atlas has been demonstrated [Caffini et al. (2010)]. Fig. 11 reports an atlas reconstruction of a cortical activation during a visual protocol of pattern reversal checkerboard.

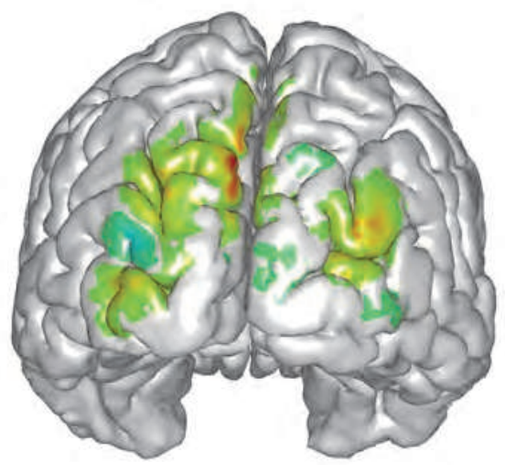

Fig. 11. Atlas map visualization of an MRI-guided optical reconstruction of the brain activation in the visual cortex (the brain is seen from the back), during a pattern reversal checkerboard protocol.

4. Conclusions

Near InfraRed Spectroscopy applied *in vivo* to cortical tissues has been widely investigated through the last two decades and big steps have been done.

From the technical point of view, the laser technology, and in particular the introduction of semiconductor laser diodes, has helped to fabricate compact and clinical instrumentations. Moreover, the improvements in light detectors has permitted to develop accurate devices, for example, in the time-resolved technology, the red-extended photocathodes well increased the quantum efficiency in the near red region.

Nevertheless, a lot more has to be done. Pulsed lasers sources are getting better and better, especially concerning time stability and output power. Photomultiplier tubes is an efficient and well established technology, but, in NIRS application, suffers the need of high voltage

supplies and the necessity to work in a dark environment, to avoid background light. Single Photon Avalanche Diodes (SPAD) are the available technology that best fits the needs of Near InfraRed Spectroscopy. Actual work is to integrate SPADs into NIRS setups by means of increased light sensitive area and better quantum efficiency in the near red spectrum. For more information about SPAD detectors see [Cova et al. (2010)].

An interesting future perspective, is the so-called null-distance measurement setup, that is the possibility to collect light from the very same point of injection. Only time resolved techniques allow this possibility and a few successful efforts have been made in this direction [Pifferi et al. (2008)].

From the medical point of view, hundreds of physiological studies and psychological tasks have been carried out and a massive literature is available on the subject. For these reason, a larger clinical use of non-invasive optical imaging in the next years is expected. In particular, we expect time resolved NIRS to be the best candidate for this purpose. The four-year nEUROPt Project [*nEUROPt Project* (2008-2012)], financed by the European Union under The Seventh Framework Programme for research and technological development (FP7) for the period 2008-2011, and coordinated by the Authors, aims at the development and clinical validation of advanced non-invasive optical methodologies for in-vivo diagnosis, monitoring, and prognosis of major neurological diseases (stroke, epilepsy, ischemia), based on diffuse optical imaging by pulsed near infrared light. The consortium plans major developments in technology and data analysis that will enhance TD-NIRS with respect to spatial resolution, sensitivity, robustness of quantification as well as performance of related instruments in clinical diagnosis and monitoring. A strong clinical basis is being produced and the diagnostic value of TD-NIRS applications to brain study will be assessed, by putting using standard methodologies (such EEG) and new optical methods side by side, in a co-registration setup. The potential commercialization of TD-NIRS systems will be then evaluated by European system manufacturers.

5. Acknowledgements

We wish to acknowledge partial support from the EC's Seventh Framework Programme (FP7/ 2007 - 2013) under grant 201076.

6. References

Arridge, S. R. (1995). Photon-measurement density functions. part i: Analytical forms, *Appl. Opt.* 34(31): 7395–7409.
URL: *http://ao.osa.org/abstract.cfm?URI=ao-34-31-7395*

Arridge, S. R. (1999). Optical tomography in medical imaging, *Inverse Problems* 15(2): R41–R93.
URL: *http://stacks.iop.org/0266-5611/15/R41*

Arridge, S. R., Dehghani, H., Schweiger, M. & Okada, E. (2000). The finite element model for the propagation of light in scattering media: A direct method for domains with nonscattering regions, *Medical Physics* 27(1): 252–264.
URL: *http://link.aip.org/link/?MPH/27/252/1*

Arridge, S. R. & Hebden, J. C. (1997). Optical imaging in medicine: Ii. modelling and reconstruction, *Physics in Medicine and Biology* 42(5): 841–853.
URL: *http://stacks.iop.org/0031-9155/42/841*

Arridge, S. R. & Schweiger, M. (1995). Photon-measurement density functions. part 2: Finite-element-method calculations, *Appl. Opt.* 34(34): 8026–8037.
URL: *http://ao.osa.org/abstract.cfm?URI=ao-34-34-8026*

Arridge, S. R., Schweiger, M., Hiraoka, M. & Delpy, D. T. (1993). A finite element approach for modeling photon transport in tissue, *Medical Physics* 20(2): 299–309.
URL: *http://link.aip.org/link/?MPH/20/299/1*

Bandettini, P., Kwong, K., Davis, T., Tootell, R., Wong, E., Fox, P., Belliveau, J., Weisskoff, R. & Rosen, B. (1997). Characterization of cerebral blood oxygenation and flow changes during prolonged brain activation, *Human Brain Mapping* 5(2): 93–109.

Becker, W. (2005). *Advanced Time-Correlated Single Photon Counting Techniques*, Springer.

Boas, D. A. (1996). *Diffuse Photon Probes of Structural and Dynamical Properties of Turbid Media: Theory and Biomedical Applications*, PhD thesis, University of Pennsylvania.

Boas, D. A. & Dale, A. M. (2005). Simulation study of magnetic resonance imaging-guided cortically constrained diffuse optical tomography of human brain function, *Appl. Opt.* 44(10): 1957–1968.
URL: *http://ao.osa.org/abstract.cfm?URI=ao-44-10-1957*

Boas, D. A., Dale, A. M. & Franceschini, M. A. (2004). Diffuse optical imaging of brain activation: approaches to optimizing image sensitivity, resolution, and accuracy, *NeuroImage* 23(Supplement 1): S275 – S288. Mathematics in Brain Imaging.

Boas, D., Culver, J., Stott, J. & Dunn, A. (2002). Three dimensional monte carlo code for photon migration through complex heterogeneous media including the adult human head, *Opt. Express* 10(3): 159–170.
URL: *http://www.opticsexpress.org/abstract.cfm?URI=oe-10-3-159*

Butti, M., Contini, D., Molteni, E., Caffini, M., Spinelli, L., Baselli, G., Bianchi, A. M., Cerutti, S., Cubeddu, R. & Torricelli, A. (2009). Effect of prolonged stimulation on cerebral hemodynamic: A time-resolved fnirs study, *Medical Physics* 36(9): 4103–4114.
URL: *http://link.aip.org/link/?MPH/36/4103/1*

Caffini, M., Torricelli, A., Cubeddu, R., Custo, A., Dubb, J. & Boas, D. A. (2010). Validating an Anatomical Brain Atlas for Analyzing NIRS Measurements of Brain Activation, *Biomedical Optics*, Optical Society of America, p. JMA87.
URL: *http://www.opticsinfobase.org/abstract.cfm?URI=BIOMED-2010-JMA87*

Caffini, M., Zucchelli, L., Contini, D., Cubeddu, R., Spinelli, L., Boas, D. & Torricelli, A. (2011). Anatomical brain atlas for nirs measurements of brain activation, *Proc. SPIE* 8088(1): 808809.

Contini, D. (2007). *Time-resolved functional Near Infrared Spectroscopy for Neuroscience*, PhD thesis, Politecnico di Milano.

Contini, D., Martelli, F. & Zaccanti, G. (1997). Photon migration through a turbid slab described by a model based on diffusion approximation. i. theory, *Appl. Opt.* 36(19): 4587–4599.
URL: *http://ao.osa.org/abstract.cfm?URI=ao-36-19-4587*

Contini, D., Spinelli, L., Torricelli, A., Pifferi, A. & Cubeddu, R. (2007). Novel method for depth-resolved brain functional imaging by time-domain nirs, *Diffuse Optical Imaging of Tissue*, Optical Society of America, p. 6629.

Cova, S., Ghioni, M., Zappa, F., Gulinatti, A., Rech, I. & Tosi, A. (2010). Single photon counting detectors in action: Retrospect and prospect, *2010 23rd Annual Meeting of the IEEE Photonics Society, PHOTINICS 2010*, pp. 177–178.
URL: *www.scopus.com*

D'Arceuil, H. E., Hotakainen, M. P., Liu, C., Themelis, G., de Crespigny, A. J. & Franceschini, M. A. (2005). Near-infrared frequency-domain optical spectroscopy and magnetic resonance imaging: a combined approach to studying cerebral maturation in neonatal rabbits, *Journal of Biomedical Optics* 10(1).

Donati, S. (1998). *Fotorivelatori*, 2a edizione edn, AEI.

Fang, Q. & Boas, D. A. (2009). Monte carlo simulation of photon migration in 3d turbid media accelerated by graphics processing units, *Optics Express* 17(22): 20178–20190.
URL: *http://www.opticsexpress.org/abstract.cfm?URI=oe-17-22-20178*

Fantini, S., Franceschini, M.-A., Maier, J. S., Walker, S. A., Barbieri, B. B. & Gratton, E. (1995). Frequency-domain multichannel optical detector for noninvasive tissue spectroscopy and oximetry, *Optical Engineering* 34(1): 32–42.
URL: *http://link.aip.org/link/?JOE/34/32/1*

Feynman, R. P., Leighton, R. B. & Sands, M. (1964). *The Feynman Lectures on Physics including Feynman's Tips on Physics: The Definitive and Extended Edition*, Addison-Wesley.

Heekeren, H. R., Obrig, H., Wenzel, R., Eberle, K., Ruben, J., Villringer, K., Kurth, R. & Villringer, A. (1997). Cerebral haemoglobin oxygenation during sustained visual stimulation – a near–infrared spectroscopy study, *Philosophical Transactions of the Royal Society of London. Series B: Biological Sciences* 352(1354): 743–750.
URL: *http://rstb.royalsocietypublishing.org/content/352/1354/743.abstract*

Ishimaru, A. (1978). *Wave Propagation and Scattering in Random Media*, Academic Press.

Jackson, J. D. (1999). *Classical Electrodynamics*, 3rd edn, Wiley.

Liebert, A., Wabnitz, H., Steinbrink, J., Obrig, H., Möller, M., Macdonald, R., Villringer, A. & Rinneberg, H. (2004). Time-resolved multidistance near-infrared spectroscopy of the adult head: Intracerebral and extracerebral absorption changes from moments of distribution of times of flight of photons, *Appl. Opt.* 43(15): 3037–3047.
URL: *http://ao.osa.org/abstract.cfm?URI=ao-43-15-3037*

Martelli, F., Bianco, S. D., Ismaelli, A. & Zaccanti, G. (2010). *Photon Migration Through Diffusive Media: Theory, Solutions and Software*, SPIE Press.

Martelli, F., Bianco, S. D. & Zaccanti, G. (2005). Perturbation model for light propagation through diffusive layered media, *Physics in Medicine and Biology* 50(9): 2159–2166.
URL: *http://stacks.iop.org/0031-9155/50/2159*

Merritt, S., Bevilacqua, F., Durkin, A. J., Cuccia, D. J., Lanning, R. & Tromberg, B. J. (2002). Near-infrared spectroscopy and mri co-registration of tumor tissue physiology, *Biomedical Topical Meeting*, Optical Society of America, p. SuE1.
URL: *http://www.opticsinfobase.org/abstract.cfm?URI=BIO-2002-SuE1*

Mie, G. (1908). Beiträge zur optik trüber medien, speziell kolloidaler metallösungen, *Annalen der Physik* 330(3): 377–445.
URL: *http://dx.doi.org/10.1002/andp.19083300302*

nEUROPt Project (2008-2012).
URL: *www.neuropt.eu*

O'Connor, D. V. & Phillips, D. (1984). *Time correlated single photon counting*, Academic Press.

Patterson, M. S., Chance, B. & Wilson, B. C. (1989). Time resolved reflectance and transmittance for the non-invasive measurement of tissue optical properties, *Appl. Opt.* 28(12): 2331–2336.
URL: *http://ao.osa.org/abstract.cfm?URI=ao-28-12-2331*

Pifferi, A., Taroni, P., Valentini, G. & Andersson-Engels, S. (1998). Real-time method for fitting time-resolved reflectance and transmittance measurements with a monte carlo model, *Appl. Opt.* 37(13): 2774–2780.
URL: *http://ao.osa.org/abstract.cfm?URI=ao-37-13-2774*

Pifferi, A., Torricelli, A., Spinelli, L., Contini, D., Cubeddu, R., Martelli, F., Zaccanti, G., Tosi, A., Mora, A. D., Zappa, F. & Cova, S. (2008). Time-resolved functional near-infrared spectroscopy at null source-detector separation, *Biomedical Optics*, Optical Society of America, p. BWC6.
URL: *http://www.opticsinfobase.org/abstract.cfm?URI=BIOMED-2008-BWC6*

Press, W. H., Teukolsky, S. A., Vetterling, W. T. & Flannery, B. P. (1992). *Numerical Recipes in C - The Art of Scientific Computing*, Cambridge University Press.

Rutherford, E. (1911). The scattering of alpha and beta particles by matter and the structure of the atom, *Philosophical Magazine Series 6* 21(125): 669–688.

Saager, R. B. & Berger, A. J. (2005). Direct characterization and removal of interfering absorption trends in two-layer turbid media, *J. Opt. Soc. Am. A* 22(9): 1874–1882.
URL: *http://josaa.osa.org/abstract.cfm?URI=josaa-22-9-1874*

Sanchez, R. & McCormick, N. J. (1982). A review of neutron transport approximations, *Nuclear Science and Engineering* 80(4): 481–535.

Sassaroli, A. & Fantini, S. (2004). Comment on the modified beer-lambert law for scattering media, *Physics in Medicine and Biology* 49(14): N255–N257.
URL: *http://stacks.iop.org/0031-9155/49/N255*

Selb, J., Stott, J. J., Franceschini, M. A., Sorensen, A. G. & Boas, D. A. (2005). Improved sensitivity to cerebral hemodynamics during brain activation with a time-gated optical system: analytical model and experimental validation, *Journal of Biomedical Optics* 10(1): 011013.
URL: *http://link.aip.org/link/?JBO/10/011013/1*

Steinbrink, J., Wabnitz, H., Obrig, H., Villringer, A. & Rinneberg, H. (2001). Determining changes in nir absorption using a layered model of the human head, *Physics in Medicine and Biology* 46(3): 879–896.
URL: *http://stacks.iop.org/0031-9155/46/879*

Strangman, G., Boas, D. A. & Sutton, J. P. (2002). Non-invasive neuroimaging using near-infrared light, *Society of Biological Psychiatry* 52: 679–693.

Torricelli, A., Contini, D., Pifferi, A., Spinelli, L., Cubeddu, R., Nocetti, L., Manginelli, A.-A. & Baraldi, P. (2007). Simultaneous acquisition of time-domain fnirs and fmri during motor activity, *Proc. SPIE* 6631(1): 66310A.
URL: *http://dx.doi.org/doi/10.1117/12.727699*

Tsuchiya, Y. (2001). Photon path distribution and optical responses of turbid media: theoretical analysis based on the microscopic beer-lambert law, *Physics in Medicine and Biology* 46(8): 2067–2084.
URL: *http://stacks.iop.org/0031-9155/46/2067*

Wabnitz, H., Liebert, A., Contini, D., Spinelli, L. & Torricelli, A. (2008). Depth selectivity in time-domain optical brain imaging based on time windows and moments of

time-of-flight distributions, *Biomedical Optics*, Optical Society of America, p. BMD9.
URL: *http://www.opticsinfobase.org/abstract.cfm?URI=BIOMED-2008-BMD9*

Wolf, M., Ferrari, M. & Quaresima, V. (2007). Progress of near-infrared spectroscopy and topography for brain and muscle clinical applications, *Journal of Biomedical Optics* 12(6): 062104.
URL: *http://link.aip.org/link/?JBO/12/062104/1*

Zege, E. P., Ivanov, A. I. & Katsev, I. L. (1991). *Image Transfer through a Scattering Medium*, Springer-Verlag.

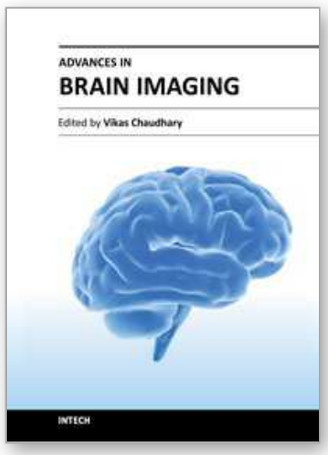

Advances in Brain Imaging

Edited by Dr. Vikas Chaudhary

ISBN 978-953-307-955-4
Hard cover, 264 pages
Publisher InTech
Published online 01, February, 2012
Published in print edition February, 2012

Remarkable advances in medical diagnostic imaging have been made during the past few decades. The development of new imaging techniques and continuous improvements in the display of digital images have opened new horizons in the study of brain anatomy and pathology. The field of brain imaging has now become a fast-moving, demanding and exciting multidisciplinary activity. I hope that this textbook will be useful to students and clinicians in the field of neuroscience, in understanding the fundamentals of advances in brain imaging.

How to reference

In order to correctly reference this scholarly work, feel free to copy and paste the following:

Matteo Caffini, Davide Contini, Rebecca Re, Lucia M. Zucchelli, Rinaldo Cubeddu, Alessandro Torricelli and Lorenzo Spinelli (2012). Functional Near Infrared Spectroscopy and Diffuse Optical Tomography in Neuroscience, Advances in Brain Imaging, Dr. Vikas Chaudhary (Ed.), ISBN: 978-953-307-955-4, InTech, Available from: http://www.intechopen.com/books/advances-in-brain-imaging/functional-near-infrared-spectroscopy-and-diffuse-optical-tomography-in-neuroscience

INTECH
open science | open minds

InTech Europe
University Campus STeP Ri
Slavka Krautzeka 83/A
51000 Rijeka, Croatia
Phone: +385 (51) 770 447
Fax: +385 (51) 686 166
www.intechopen.com

InTech China
Unit 405, Office Block, Hotel Equatorial Shanghai
No.65, Yan An Road (West), Shanghai, 200040, China
中国上海市延安西路65号上海国际贵都大饭店办公楼405单元
Phone: +86-21-62489820
Fax: +86-21-62489821

IntechOpen